THE JOURNAL OF PHYSICAL CHEMISTRY Letters

Letter

pubs.acs.org/JPCL

Radiative and Nonradiative Recombination in $CuInS_2$ Nanocrystals and $CuInS_2$-Based Core/Shell Nanocrystals

Anne C. Berends,[‡] Freddy T. Rabouw,[‡,§] Frank C. M. Spoor,[†] Eva Bladt,[#] Ferdinand C. Grozema,[†] Arjan J. Houtepen,[†] Laurens D. A. Siebbeles,[†] and Celso de Mello Donegá*[,‡]

[‡]Condensed Matter and Interfaces, Debye Institute for Nanomaterials Science, Utrecht University, P.O. Box 80 000, 3508 TA Utrecht, The Netherlands

[†]Optoelectronic Materials Section, Department of Chemical Engineering, Delft University of Technology, Van der Maasweg 9, 2629 HZ Delft, The Netherlands

[#]Electron Microscopy for Materials Science (EMAT), University of Antwerp, Groenenborgerlaan 171, B-2020 Antwerp, Belgium

Supporting Information

ABSTRACT: Luminescent copper indium sulfide (CIS) nanocrystals are a potential solution to the toxicity issues associated with Cd- and Pb-based nanocrystals. However, the development of high-quality CIS nanocrystals has been complicated by insufficient knowledge of the electronic structure and of the factors that lead to luminescence quenching. Here we investigate the exciton decay pathways in CIS nanocrystals using time-resolved photoluminescence and transient absorption spectroscopy. Core-only CIS nanocrystals with low quantum yield are compared to core/shell nanocrystals (CIS/ZnS and CIS/CdS) with higher quantum yield. Our measurements support the model of photoluminescence by radiative recombination of a conduction band electron with a localized hole. Moreover, we find that photoluminescence quenching in low-quantum-yield nanocrystals involves initially uncoupled decay pathways for the electron and hole. The electron decay pathway determines whether the exciton recombines radiatively or nonradiatively. The development of high-quality CIS nanocrystals should therefore focus on the elimination of electron traps.

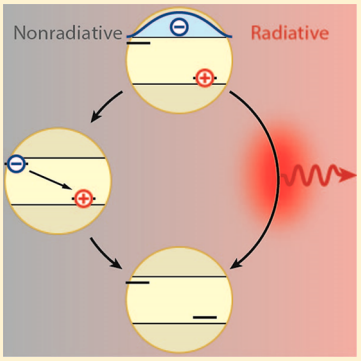

Semiconductor nanocrystals (NCs) show intriguing opto-electronic properties that differ from bulk and depend on the size and shape of the NC.[1,2] Cadmium and lead chalcogenide NCs are the most extensively studied photo-luminescent semiconductor NCs, showing emission in the visible and near-infrared spectral window. However, their utilization in consumer products is limited by toxicity concerns. This has motivated increasing research effort into compositions based on less toxic elements while possessing similar properties. Copper indium sulfide ($CuInS_2$, CIS) NCs show size-dependent photoluminescence (PL) in the red to near-infrared spectral window and large absorption coefficients and are therefore a promising alternative for lead or cadmium chalcogenide NCs in applications such as light-emitting diodes,[3−5] photovoltaics,[6−8] luminescent solar concentrators,[9,10] and bioimaging.[11,12] However, the low PL quantum yields (QYs) of bare CIS NCs (typically below 5%)[13] preclude their direct application. Improvement of the PL QYs can be achieved by overcoating the NCs with a shell of wide band gap semiconductors.[1,9,14−17] To date, the best results have been reported for CIS/CdS core/shell NCs, which show PL QYs up to 86%,[9,14] while for CIS/ZnS core/shell NCs, PL QYs up to 70% have been reported.[14,18] Alternative strategies to obtain high PL QY CIS-based core/shell NCs employing exclusively cadmium-free materials are desired but have not yet been devised. In fact, while in the well-known lead and cadmium chalcogenide NCs (e.g., PbSe and CdSe) the PL originates from radiative recombination of a delocalized electron in the conduction band (CB) with a delocalized hole in the valence band (VB), the origin of PL in CIS NCs is still under debate.[13,19] A commonly invoked mechanism to explain the intriguing characteristics of the PL of CIS NCs (viz., broad bandwidths of ∼200−300 meV, long lifetimes of hundreds of nanoseconds, and large Stokes shifts of ∼300−400 meV) is donor−acceptor pair recombination involving native point defects,[17,20−23] which is based on the assumption that the exciton radiative recombination mechanisms in nanoscale and bulk CIS are the same. This model does however not explain the size dependence of the PL energies, which follow the same trend as that observed for the absorption transitions. Other models involve one localized charge carrier, either the electron[19,24−26] or the hole,[14,27,28] that recombines radiatively with the remaining delocalized charge carrier. Yet another model was recently proposed, which precludes the involvement of localized carriers, ascribing the PL to the recombination of CB electron states with dark and bright VB hole states.[29] To make the next step in the improvement of the PL QY of CIS

Received: July 28, 2016
Accepted: August 23, 2016
Published: August 23, 2016

DOI: 10.1021/acs.jpclett.6b01668
J. Phys. Chem. Lett. 2016, 7, 3503−3509

NCs, a better understanding of the nature of the emitting state and of the prevailing efficiency-limiting processes is needed. As recent publications showed that the PL characteristics of copper-doped II−VI semiconductor quantum dots are very similar to those of CIS NCs,[28,30,31] a better understanding of excited-state dynamics in CIS NCs would also provide insight into the optoelectronic properties of copper-doped semiconductor NCs.

In this work, we study the excited-state dynamics in CIS core and core−shell NCs using transient absorption (TA) and time-resolved PL spectroscopy. We compare bare CIS NCs with a relatively low QY (2%) to core/shell NCs with higher QY (CIS/ZnS, 29%; and CIS/CdS, 86%), aiming at a better understanding of the competition between radiative and nonradiative decay pathways that lead to the differences in QY. (see the Supporting Information (SI), Methods, for details). The CIS core NCs have a chalcopyrite crystal structure and a trigonal pyramidal shape with a base of 2.5 ± 0.4 nm and height of 2.4 ± 0.3 nm (SI, Figure S1A). The featureless absorption spectrum extends to ∼650 nm, while the broad PL peak is centered at 660 nm with a full width at half-maximum (fwhm) of 300 meV, corresponding to a Stokes shift of 436 meV (Figure 1A and SI, Figure S2). The NC shape is preserved after CdS shell overgrowth, while the size increases (base: 3.1 ± 0.4 nm; height: 3.0 ± 0.3 nm; Figure S1B). This corresponds to a shell thickness of 1 monolayer. The PL and absorption spectra shift to higher energies upon shell overgrowth, for both ZnS and CdS shells (Figure 1A). A blue shift of the optical transitions is commonly observed after ZnS overcoating of CIS NCs and also in the early stages of CdS shell growth on CIS NCs[14] but is nevertheless not yet well-understood. It has been ascribed to alloying,[15,16,32−36] size reduction due to cation exchange[37] or etching,[14,34,37] interfacial strain,[38] and surface reconstruction.[39] Shell overgrowth is observed to greatly improve the PL QY, from 2% for the CIS NCs to 29% for CIS/ZnS NCs and 86% for CIS/CdS NCs. The PL lifetimes become longer with increasing QY (Figure 1B), indicating that nonradiative recombination pathways in core NCs are (partially) removed upon shell growth.[14,15,32] In contrast, the Stokes shift and PL bandwidth are hardly affected by the shell overgrowth (Figure 1 and SI, Figure S2). This indicates that the electronic transitions observed in the optical spectra of bare and core/shell CIS NCs are the same.

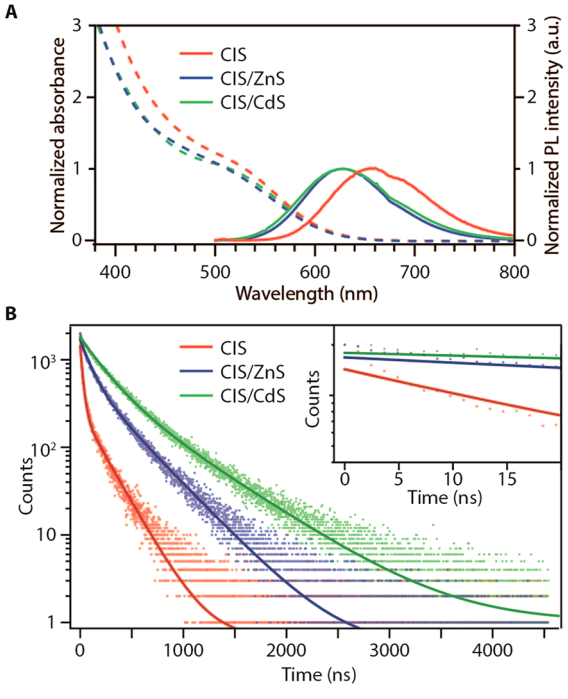

Figure 1. (A) Steady-state absorption (dashed lines) and PL (solid lines) spectra of CIS NCs (red), CIS/ZnS core/shell NCs (blue), and CIS/CdS core/shell NCs (green). PL excitation spectra are shown in the SI, Figure S2. (B) PL decay curves of the three samples (data points), fitted with a biexponential function (solid lines). The fits yield decay constants of 25 and 207 ns for CIS core NCs, 201 and 357 ns for CIS/ZnS NCs, and 209 and 566 ns for CIS/CdS NCs. The inset shows a zoom-in on the first 20 ns.

Using TA spectroscopy, we look more closely at the subnanosecond quenching processes taking place in the NCs after excitation. The NCs dispersed in hexane are excited with a short (170 fs) pump laser pulse at 500 nm, after which a broadband probe pulse (350−1600 nm) at variable time delay records changes in the NC absorption spectrum. The different processes relevant to the TA experiments carried out in this work are schematically shown in Figure S3 (SI). Figure 2A shows TA spectral slices (two-dimensional TA images are shown in the SI, Figure S4) for CIS NCs for pump−probe delay times between 1 ps and 2 ns. A negative signal (i.e., a photoinduced reduction in absorption) appears at around 530 nm, at the same wavelength as the shoulder in the steady-state absorption spectrum (Figure 1A and SI, Figure S7). This signal is therefore assigned to the band edge bleach, in agreement with previous reports.[25,27,40−43] In the infrared (700−1600 nm), a broad positive signal is observed. We assign this to excited-state absorption and will discuss its possible nature in more detail below. The observation of photoinduced absorption in CIS NCs is consistent with previous TA measurements in the red and near-infrared,[25,40] and the data presented here reveal the true magnitude of this TA spectral feature. Both the positive and negative signals decay partially on the nanosecond time scale investigated. The TA spectral slices of CIS/ZnS NCs (Figure 2B and SI, Figure S5) are qualitatively similar to those for the bare CIS NCs. Again, we observe a decaying band edge bleach signal at 530 nm and a broad decaying excited-state absorption signal. The situation is different in CIS/CdS NCs (Figure 2C and SI, Figure S6). The band edge bleach and excited-state absorption signals are observed as well, but they hardly decay on the nanosecond time scale investigated here. While the band edge bleach persists over (at least) the first 3 ns, the PL decay trace of CIS/CdS NCs shows no rise on a nanosecond time scale (Figure 1B). We therefore exclude the donor−acceptor pair recombination model because in this model the PL should originate from two trapped charge carriers, which would not produce a band edge bleach signal, in clear contradiction with our observations.

Recent work by Knowles et al.[28] and Rice et al.[31] reported the observation of magnetic circularly polarized luminescence in CIS NCs. Both groups concluded that the PL in CIS NCs originates from radiative recombination of a delocalized electron with a localized hole, in agreement with previous reports,[14,42] and proposed that the hole localizes, specifically, on a Cu ion.[28,31] However, on the basis of the observation of magnetic circular dichroism spectra, the authors of ref 31 conclude that paramagnetic Cu^{2+} ions are already present in the CIS NCs prior to photoexcitation, while ref 28 proposes that paramagnetic Cu^{2+} ions are only formed after photoexcitation,

DOI: 10.1021/acs.jpclett.6b01668
J. Phys. Chem. Lett. 2016, 7, 3503−3509

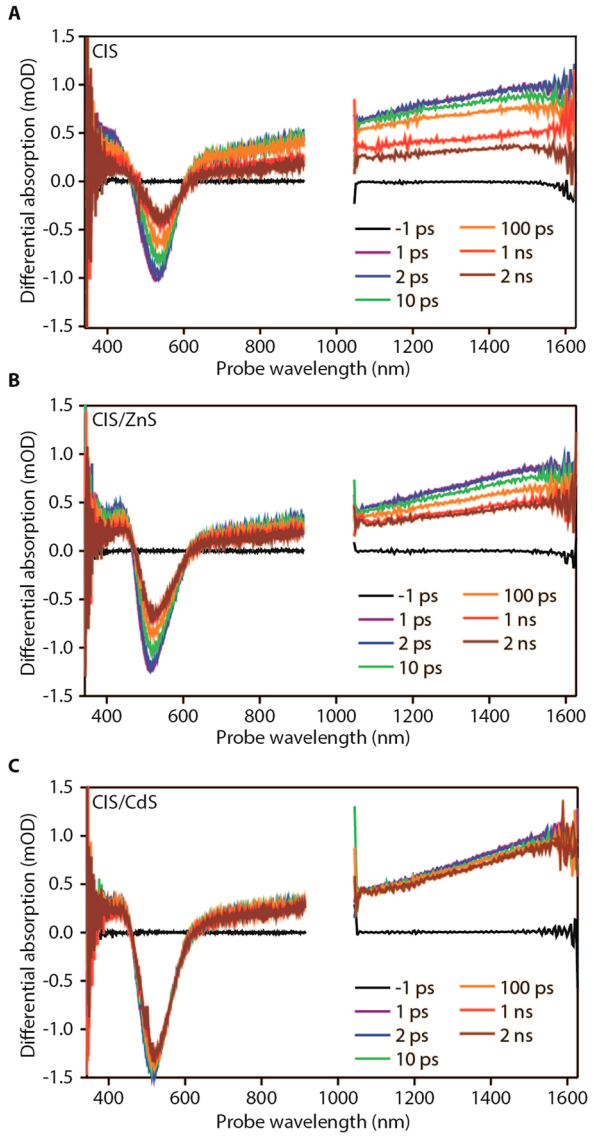

Figure 2. Spectral slices of TA measurements of the three samples (pump wavelength: 500 nm; fluence: 2.2 × 10^{13} photons/cm^2): (A) CIS NCs, (B) CIS/ZnS NCs, and (C) CIS/CdS NCs. 2D TA spectra are provided in the SI (Figures S4–S6).

upon localization of a photogenerated hole on a Cu^+ ion. As will be discussed below, our observations are not consistent with the presence of ground-state Cu^{2+} ions and therefore support the latter scenario. We assign the band edge bleach observed in our TA data (Figure 2) to the electron in the lowest-energy delocalized CB state. Indeed, previous work by Li et al.[14] has shown that the state responsible for the ground-state bleach in the TA spectra of CIS NCs has a two-fold degeneracy, consistent with an electron state.[44] We attribute the excited-state absorption to the hole localized on a Cu atom. The signal could be due to ligand-to-metal charge-transfer transitions where the hole is excited to a VB level.[30] This type of transition is expected to strongly couple to phonons. Moreover, the degeneracy of the VB is high.[44] This explains why the excited-state absorption band is broad and featureless. Note that intraband absorption transitions between CB states, on the other hand, would be expected to show up as well-defined peaks in the mid-infrared at around 2000 nm[45] because there is a single CB in $CuInS_2$ with an effective electron mass similar to that in CdSe.[29,44,46] We do not observe these transitions due to the limited spectral range covered in our TA experiments. Interestingly, in the steady-state absorption spectrum, none of the samples shows any significant absorption in the 800–1600 nm range (SI, Figure S8). Moreover, laser excitation with sub-band-gap energy does not induce any observable TA signal. This implies that localized holes and/or excess carriers are either absent or have negligible concentrations prior to the photogeneration of excitons. We must therefore conclude that copper ions are monovalent in the NC ground state, while Cu^{2+} forms only after capture of a photogenerated hole. This observation is inconsistent with the model proposed in ref 31.

The TA decay dynamics of the three samples are shown in Figure 3A–C, normalized to the signal at 2.5 ns. In the analysis, we can neglect effects of Auger recombination of multiexciton states because the estimated number of excitons per NC per laser pulse is $\langle N_0 \rangle$ = 0.03 (SI, Figures S9 and S10). The dynamics of the band edge bleach (averaged from 540 to 570 nm; ascribed to CB electrons) are plotted in blue, and those of the excited-state absorption (averaged from 750 to 800 nm; ascribed to localized holes) are in red. The raw data (i.e., prior to normalization, Figure 4A–C) show that the signal from the delocalized electron (blue) is approximately four times stronger

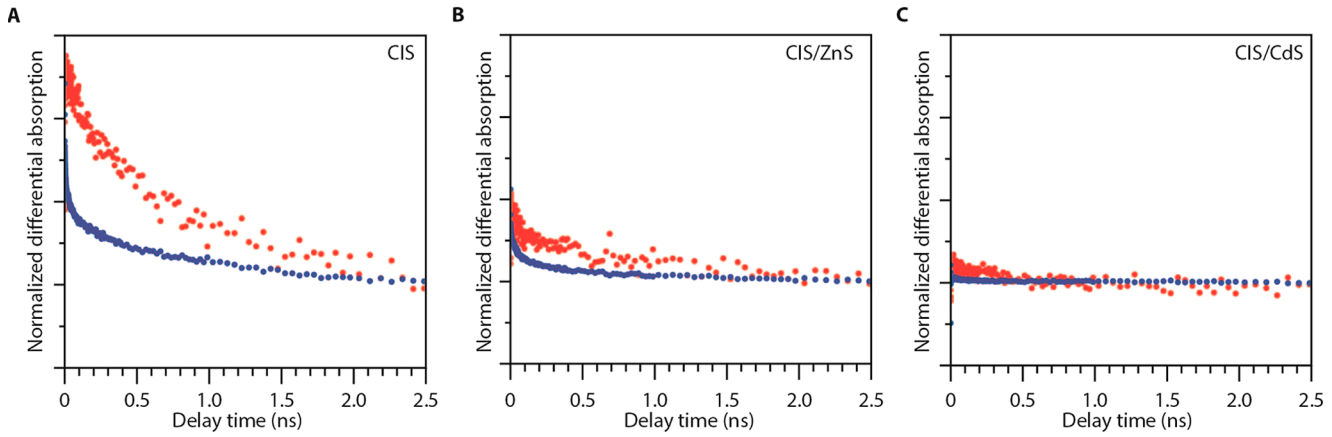

Figure 3. Comparison of the dynamics of the band edge bleach (blue) and excited-state absorption (red) signals for the three samples: CIS core NCs (A), CIS/ZnS core/shell NCs (B), and CIS/CdS core/shell NCs (C). Both the excited-state absorption and the band edge bleach signal are normalized to the signal at t = 2.5 ns.

DOI: 10.1021/acs.jpclett.6b01668
J. Phys. Chem. Lett. 2016, 7, 3503–3509

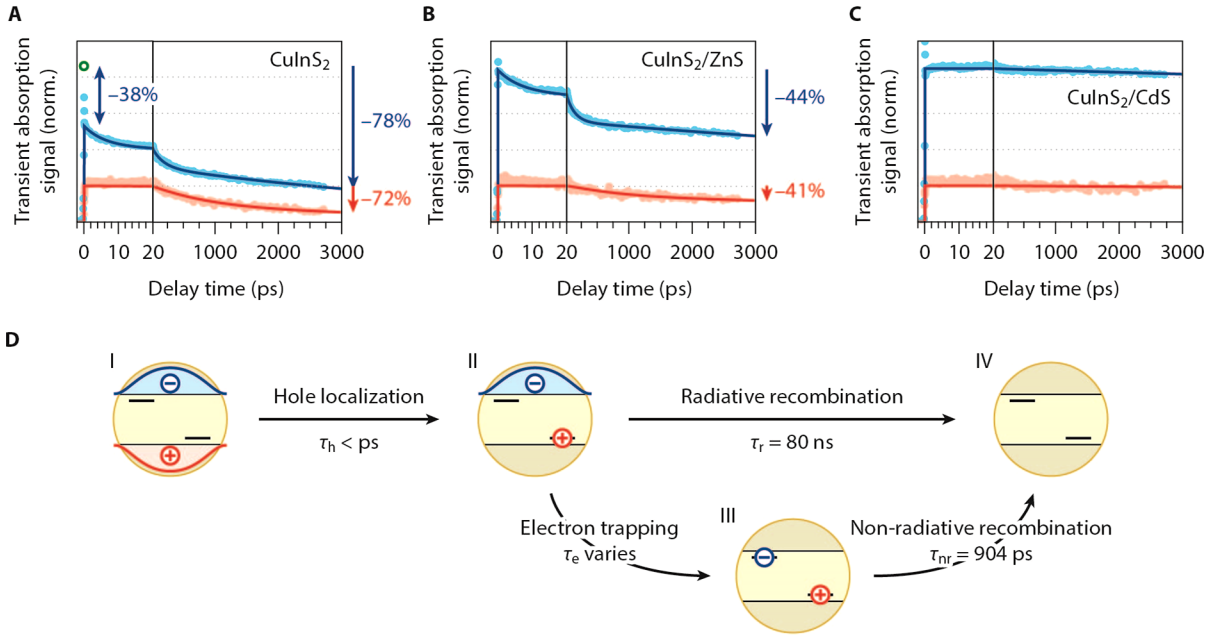

Figure 4. (A–C) Decay dynamics of the TA signals, with the band edge bleach signal in blue and the excited-state absorption in red. The solid lines are fits of our model to the lighter colored data points. Both the excited-state absorption (red) and the band edge bleach (blue) are normalized to the signal amplitude of the excited-state absorption (red) at $t = 0$. The green circle in panel A is the initial amplitude of the band edge bleach in the absence of ultrafast electron trapping (see the main text for discussion). (D) Schematic representation of the model proposed. After photoexcitation creating an exciton, there is fast localization of the hole. A distribution of electron trapping rates makes the TA signal decay multiexponential. A trapped electron recombines nonradiatively with the localized hole, while a delocalized electron recombines radiatively with the localized hole. The fitted "radiative lifetime" of 80 ns, based on the data on CIS/CdS NCs, is a rough estimate and cannot be determined accurately because our TA experiment has a too short time range (see also Figure 1). The fitted time constants for electron trapping are 6.1 ± 1.1 ps (with a contribution of 21.3 ± 0.4%), 173 ± 5 ps (21.0 ± 0.3%), and 6.0 ± 0.4 ns (57.7 ± 0.2%) for CIS core NCs and 6.4 ± 0.5 ps (13.9 ± 0.5%), 129 ± 3 ps (19.9 ± 0.3%), and 19.2 ± 0.8 ns (66.2 ± 0.1%) for CIS/ZnS. The time constant for nonradiative recombination of the trapped electron with a localized hole is 905 ± 33 ps, obtained from a global fit to the excited-state absorption transients. The ratio of excited-state absorption and ground-state bleach cross sections is 0.236 ± 0.002. See the SI for more details of the model and the fitting procedure.

than that from the localized hole (red) because the transitions probed have different cross sections. For the CIS core NCs, the initial signal intensity at $t = 0$ from the delocalized electron is relatively weak (significantly less than four times stronger than the hole signal). This points to ultrafast electron trapping in some NCs on subpicosecond time scales that cannot be resolved in our TA experiment. Without ultrafast electron trapping, the initial bleach signal in CIS NCs at $t = 0$ would be at the green circle in Figure 4A.

The decay dynamics of the populations of CB electrons (blue) and localized holes (red) are different on the picosecond time scale, as most clearly visible in the normalized data (Figure 3A–C). The electron population decays more rapidly than the hole population in CIS and CIS/ZnS. However, the intensity ratio of electron and hole signals at a delay time of 2.5 ns is the same for the three samples (Figure 4A–C). This means that the electron and hole decay pathways are separate on a picosecond time scale but eventually couple on a nanosecond time scale. Indeed, for CIS/ZnS, the electron and hole populations drop by 44 and 41% over the first 2.5 ns (Figure 4B), respectively, and in CIS/CdS, they drop by 4 and 4% (Figure 4C). In CIS core NCs, the drops in electron and hole populations are 72 and 78% (Figure 4A) if we take into account the effect of ultrafast electron trapping (see above). We conclude that the overall decay of electron and hole populations over 2.5 ns must be due to recombination (radiative and/or nonradiative), which explains why the signal ratio at 2.5 ns is the same for the three samples. We ascribe the fast picosecond dynamics of the bleach signal in CIS and CIS/ZnS NCs to trapping of CB electrons. Indeed, trapping of the CB electron would make it unobservable in our TA experiment, while this process does not immediately affect the hole population. Subsequently, trapped electrons recombine nonradiatively with the hole on a nanosecond time scale, eventually leading to the observation of coupled populations. Interestingly, the drops in population over 2.5 ns show an inverse correlation with the PL QYs of the samples, confirming that the subnanosecond charge carrier dynamics reflect nonradiative recombination pathways.

These observations are used to build a simple kinetic model (Figure 4D) for the charge carrier dynamics and nonradiative recombination pathway in CIS NCs. It involves ultrafast (subpicosecond) localization of the hole, as evidenced by the absence of a clear rise in the excited-state absorption signal over the instrument response of our setup. Likewise, the electron reaches the lowest CB state on subpicosecond time scales. The resulting situation is schematically depicted in Figure 4D, state II. In some NCs, the electron is subsequently trapped on picosecond–nanosecond time scales, giving rise to a fast component in the band edge bleach decay dynamics, resulting in state III. A trapped electron recombines nonradiatively with the localized hole, resulting in the approximate nanosecond decay dynamics of the excited-state absorption (process III to IV). When the electron is not trapped, it recombines radiatively with the localized hole (process II to IV) on nanosecond–microsecond time scales.

DOI: 10.1021/acs.jpclett.6b01668
J. Phys. Chem. Lett. 2016, 7, 3503–3509

Our model matches the observed TA dynamics for all three samples well. The solid lines in Figure 4A–C are the result of a global fit of the TA dynamics of the three samples (see the SI for details). The good match confirms that electron trapping is the first step in the nonradiative recombination pathway in CIS-based NCs (states II–III in Figure 4D). The multiexponential electron dynamics in the CIS and CIS/ZnS NCs are modeled using three NC populations with different electron trapping rates[47] plus a fourth population with ultrafast trapping for the CIS NCs. Next, the hole dynamics are reproduced for all three samples with the addition of a single additional fit parameter, namely, the nonradiative recombination rate of a trapped electron with a localized hole (states III–IV). The nonradiative recombination has a fixed rate constant of $1/(905 \pm 33$ ps) for the three samples. However, the probability and the moment that nonradiative recombination occurs varies because it is only the second step in the process after electron trapping. This means that electron trapping is the primary cause for nonradiative recombination in CIS-based NCs, determining the overall rate and probability. We find the same results on data obtained using shorter-wavelength excitation (SI, Figure S11), confirming the robustness of our model.

The model presented here provides important new insights into the *nonradiative* decay pathways of electrons and holes in CIS-based NCs. At the same time, it confirms recent models for the nature of *radiative* decay in these NCs.[28,31] Radiative decay (state II to state IV in Figure 4D) is due to recombination of a hole localized on a Cu ion with a CB electron. This explains the intriguing characteristics of PL in CIS-based NCs and copper-doped NCs. Radiative lifetimes are long (Figure 1B) because the wave function overlap of a delocalized CB electron with a localized hole is relatively small. Furthermore, the large apparent Stokes shift and broad emission bands are due to energy relaxation upon localization of the hole, variations in the electronic environment of Cu,[48] and coupling to vibrations. Indeed, strong vibrational coupling is expected for transitions with a charge-transfer character (the localized hole effectively oxidizes a Cu^+ ion to Cu^{2+}) because they are accompanied by changes in metal-to-ligand bond length.[28,49] Moreover, our observations are consistent with the localization of the photogenerated hole on a Cu^+ ion, in agreement with a recently proposed mechanism.[28] However, we note that our work does not allow any conclusion regarding the nature of the hole localization process (i.e., self-trapping onto a regular Cu^+ ion, as proposed by Knowles et al.,[28] or capture by a native defect, such as a Cu^+ ion on an In^{3+} site). The recently demonstrated similarity between the optical properties of CIS NCs and Cu-doped semiconductor NCs[28,30,31] may be interpreted as indication that antisite defects (i.e., Cu_{In}'') are relevant because Cu^+ doped in II–VI (e.g., CdSe or ZnSe) or III–V (e.g., InP) semiconductor NCs also occupies heterovalent sites (e.g., Cu_{Cd}' or Cu_{In}''). Nevertheless, the unambiguous identification of the hole localization sites in CIS NCs will require sophisticated techniques, such as electron spin echo detected electron paramagnetic resonance (ESE-EPR) and electron–nuclear double resonance (ENDOR) spectroscopies. ESE-EPR and ENDOR spectroscopies have been successfully used to identify the nature of donors and acceptors in Li-doped ZnO quantum dots[50,51] and could also shed light on the hole localization process in CIS NCs.

The results presented above show that electron trapping leading to nonradiative decay is most effectively blocked by growing a CdS shell around CIS NCs. The shells used in the present study are too thin (viz., 1 monolayer) to significantly affect the carrier localization regime (type-I versus type-II).[1] Their impact on the electron recombination pathways therefore most likely results from differences in their ability to eliminate electron traps at the CIS surface. The lattice mismatch is 2% between CIS and ZnS (lattice parameters a,b = 5.52279 Å for CIS,[52] and a,b,c = 5.41450 Å for ZnS[53]) and 5.2% between CIS and CdS (a,b,c = 5.81000 for CdS[54]). The small lattice mismatch between CIS and ZnS, in combination with the high diffusion rates in CIS,[55] might favor interdiffusion and alloy formation, which would result in some surface Cu and In atoms, thereby preventing the complete elimination of CIS-related surface traps. In contrast, the larger mismatch between CIS and CdS would prevent interdiffusion, facilitating the formation of a CIS/CdS core/shell architecture, in which the surface of the NCs would be devoid of CIS units and therefore of CIS-related surface traps.

In conclusion, we have carried out detailed analysis of the TA dynamics of the band edge bleach and excited-state absorption signals of CIS core NCs, CIS/ZnS core/shell NCs, and CIS/CdS core/shell NCs. On the basis of this analysis, we propose a model that describes two exciton recombination pathways in CIS and CIS-based NCs, one leading to nonradiative decay and the other to radiative decay. The radiative decay originates from recombination of a delocalized electron to a Cu-localized hole, explaining the large apparent Stokes shift and the long PL lifetimes. Electron trapping, probably on the surface of the CIS NCs, is the first step of the nonradiative recombination pathway. Removing these traps leads to improvement of the PL QY of CIS-based core/shell NCs.

■ ASSOCIATED CONTENT

Supporting Information

The Supporting Information is available free of charge on the ACS Publications website at DOI: 10.1021/acs.jpclett.6b01668.

Experimental methods; HAADF-STEM images of the CIS core NCs and CIS/CdS core/shell NCs; PL, absorption, and PL excitation spectra of the CIS core NCs and CIS/ZnS core/shell and CIS/CdS core/shell NCs; schematic representation of different processes that can take place in TA spectroscopy experiments; 2D TA images of CIS core NCs, CIS/ZnS core/shell NCs, and CIS/CdS core/shell NCs; TA, steady-state absorption, and PL spectra in one graph; steady-state absorption spectra of the NC solutions used for the TA measurements; power-dependent ground-state bleach decay curves and fits of the three samples; normalized power-dependent ground-state bleach decay curves; calculation of the average number of excitons per NC; and model description and global fit details (PDF)

■ AUTHOR INFORMATION

Corresponding Author

*E-mail: c.demello-donega@uu.nl.

Present Address

§F.T.R.: Department of Mechanical and Process Engineering, ETH Zürich, Leonhardstrasse 21, 8092 Zürich, Switzerland.

Notes

The authors declare no competing financial interest.

DOI: 10.1021/acs.jpclett.6b01668
J. Phys. Chem. Lett. 2016, 7, 3503–3509

■ ACKNOWLEDGMENTS

The authors thank Sara Bals (EMAT, Antwerp) for fruitful discussions and Chenghui Xia for providing the fluorophore Lumogen red 305 for the PL QY measurements. A.C.B. and C.d.M.D. acknowledge financial support from the division of Chemical Sciences (CW) of The Netherlands Organization for Scientific Research (NWO) under Grant Number ECHO.712.014.001. E.B. gratefully acknowledges financial support by the Flemish Fund for Scientific Research (FWO Vlaanderen). This research was supported by the Dutch Foundation for Fundamental Research on Matter (FOM) in the program "Hot Electrons in Cool Nanocrystals".

■ REFERENCES

(1) Donega, C. d. M. Synthesis and Properties of Colloidal Heteronanocrystals. *Chem. Soc. Rev.* **2011**, *40*, 1512−1546.
(2) Kovalenko, M. V.; Manna, L.; Cabot, A.; Hens, Z.; Talapin, D. V.; Kagan, C. R.; Klimov, V. I.; Rogach, A. L.; Reiss, P.; Milliron, D. J.; et al. Prospects of Nanoscience with Nanocrystals. *ACS Nano* **2015**, *9*, 1012−1057.
(3) Yoon, H. C.; Oh, J. H.; Ko, M.; Yoo, H.; Do, Y. R. Synthesis and Characterization of Green Zn−Ag−In−S and Red Zn−Cu−In−S Quantum Dots for Ultrahigh Color Quality of Down-Converted White LEDs. *ACS Appl. Mater. Interfaces* **2015**, *7*, 7342−7350.
(4) Demir, N.; Oner, I.; Varlikli, C.; Ozsoy, C.; Zafer, C. Efficiency Enhancement in a Single Emission Layer Yellow Organic Light Emitting Device: Contribution of CIS/ZnS Quantum Dot. *Thin Solid Films* **2015**, *589*, 153−160.
(5) Park, S. H.; Hong, A.; Kim, J.-H.; Yang, H.; Lee, K.; Jang, H. S. Highly Bright Yellow-Green-Emitting $CuInS_2$ Colloidal Quantum Dots with Core/Shell/Shell Architecture for White Light-Emitting Diodes. *ACS Appl. Mater. Interfaces* **2015**, *7*, 6764−6771.
(6) Chang, J.-Y.; Su, L.-F.; Li, C.-H.; Chang, C.-C.; Lin, J.-M. Efficient "Green" Quantum Dot-Sensitized Solar Cells Based on Cu_2S−$CuInS_2$−ZnSe Architecture. *Chem. Commun.* **2012**, *48*, 4848−4850.
(7) Pan, Z.; Mora-Sero, I.; Shen, Q.; Zhang, H.; Li, Y.; Zhao, K.; Wang, J.; Zhong, X.; Bisquert, J. High-Efficiency "Green" Quantum Dot Solar Cells. *J. Am. Chem. Soc.* **2014**, *136*, 9203−9210.
(8) Dunst, S.; Rath, T.; Reichmann, A.; Chien, H.; Friedel, B.; Trimmel, G. A Comparison of Copper Indium Sulfide Polymer Nanocomposite Solar Cells in Inverted and Regular Device Architecture. *Synth. Met.* **2016**, DOI: 10.1016/j.synthmet.2016.04.003.
(9) Knowles, K. E.; Kilburn, T. B.; Alzate, D. G.; McDowall, S.; Gamelin, D. R. Bright $CuInS_2$/CdS Nanocrystal Phosphors for High-Gain Full-Spectrum Luminescent Solar Concentrators. *Chem. Commun.* **2015**, *51*, 9129−9132.
(10) Meinardi, F.; McDaniel, H.; Carulli, F.; Colombo, A.; Velizhanin, K. A.; Makarov, N. S.; Simonutti, R.; Klimov, V. I.; Brovelli, S. Highly Efficient Large-Area Colourless Luminescent Solar Concentrators Using Heavy-Metal-Free Colloidal Quantum Dots. *Nat. Nanotechnol.* **2015**, *10*, 878−885.
(11) Guo, W.; Sun, X.; Jacobson, O.; Yan, X.; Min, K.; Srivatsan, A.; Niu, G.; Kiesewetter, D. O.; Chang, J.; Chen, X.; et al. Intrinsically Radioactive [^{64}Cu]CuInS/ZnS Quantum Dots for PET and Optical Imaging: Improved Radiochemical Stability and Cerenkov Luminescence. *ACS Nano* **2015**, *9*, 488−495.
(12) Chen, C.-W.; Wu, D.-Y.; Chan, Y.-C.; Lin, C. C.; Chung, P.-H.; Hsiao, M.; Liu, R.-S. Evaluations of the Chemical Stability and Cytotoxicity of $CuInS_2$ and $CuInS_2$/ZnS Core/Shell Quantum Dots. *J. Phys. Chem. C* **2015**, *119*, 2852−2860.
(13) van der Stam, W.; Berends, A. C.; de Mello Donegá, C. Prospects of Colloidal Copper Chalcogenide Nanocrystals. *ChemPhysChem* **2016**, *17*, 559−581.
(14) Li, L.; Pandey, A.; Werder, D. J.; Khanal, B. P.; Pietryga, M.; Klimov, V. I. Efficient Synthesis of Highly Luminescent Copper Indium Sulfide-Based Core/Shell Nanocrystals with Surprisingly Long-Lived Emission. *J. Am. Chem. Soc.* **2011**, *133*, 1176−1179.
(15) De Trizio, L.; Prato, M.; Genovese, A.; Casu, A.; Povia, M.; Simonutti, R.; Alcocer, M. J. P.; D'Andrea, C.; Tassone, F.; Manna, L. Strongly Fluorescent Quaternary Cu−In−Zn−S Nanocrystals Prepared from $Cu_{1-x}InS_2$ Nanocrystals by Partial Cation Exchange. *Chem. Mater.* **2012**, *24*, 2400−2406.
(16) Feng, J.; Sun, M.; Yang, F.; Yang, X. A Facile Approach to Synthesize High-Quality $Zn_{(x)}Cu_{(y)}InS_{(1.5+x+0.5y)}$ Nanocrystal Emitters. *Chem. Commun.* **2011**, *47*, 6422−6424.
(17) Seo, J.; Raut, S.; Abdel-Fattah, M.; Rice, Q.; Tabibi, B.; Rich, R.; Fudala, R.; Gryczynski, I.; Gryczynski, Z.; Kim, W.-J.; et al. Time-Resolved and Temperature-Dependent Photoluminescence of Ternary and Quaternary Nanocrystals of $CuInS_2$ with ZnS Capping and Cation Exchange. *J. Appl. Phys.* **2013**, *114*, 094310.
(18) Kim, Y.-K.; Ahn, S.-H.; Chung, K.; Cho, Y.-S.; Choi, C.-J. The Photoluminescence of $CuInS_2$ Nanocrystals: Effect of Non-Stoichiometry and Surface Modification. *J. Mater. Chem.* **2012**, *22*, 1516−1520.
(19) Leach, A. D. P.; Macdonald, J. E. The Optoelectronic Properties of $CuInS_2$ Nanocrystals and Their Origin. *J. Phys. Chem. Lett.* **2016**, *7*, 572−583.
(20) Chen, B.; Zhong, H.; Zhang, W.; Tan, Z.; Li, Y.; Yu, C.; Zhai, T.; Bando, Y.; Yang, S.; Zou, B. Highly Emissive and Color-Tunable $CuInS_2$-Based Colloidal Semiconductor Nanocrystals: Off-Stoichiometry Effects and Improved Electroluminescence Performance. *Adv. Funct. Mater.* **2012**, *22*, 2081−2088.
(21) Zhong, H.; Zhou, Y.; Ye, M.; He, Y.; Ye, J.; He, C.; Yang, C.; Li, Y. Controlled Synthesis and Optical Properties of Colloidal Ternary Chalcogenide $CuInS_2$ Nanocrystals. *Chem. Mater.* **2008**, *20*, 6434−6443.
(22) Castro, S. L.; Bailey, S. G.; Raffaelle, R. P.; Banger, K. K.; Hepp, A. F. Synthesis and Characterization of Colloidal $CuInS_2$ Nanoparticles from a Molecular Single-Source Precursor. *J. Phys. Chem. B* **2004**, *108*, 12429−12435.
(23) Nam, D. E.; Song, W. S.; Yang, H. Noninjection, One-Pot Synthesis of Cu-Deficient $CuInS_2$/ZnS Core/Shell Quantum Dots and Their Fluorescent Properties. *J. Colloid Interface Sci.* **2011**, *361*, 491−496.
(24) Omata, T.; Nose, K.; Kurimoto, K.; Kita, M. Electronic Transition Responsible for Size-Dependent Photoluminescence of Colloidal $CuInS_2$ Quantum Dots. *J. Mater. Chem. C* **2014**, *2*, 6867−6872.
(25) Kraatz, I. T.; Booth, M.; Whitaker, B. J.; Nix, M. G. D.; Critchley, K. Sub-Bandgap Emission and Intraband Defect-Related Excited-State Dynamics in Colloidal $CuInS_2$/ZnS Quantum Dots Revealed by Femtosecond Pump − Dump − Probe Spectroscopy. *J. Phys. Chem. C* **2014**, *118*, 24102−24109.
(26) Hamanaka, Y.; Kuzuya, T.; Sofue, T.; Kino, T.; Ito, K.; Sumiyama, K. Defect-Induced Photoluminescence and Third-Order Nonlinear Optical Response of Chemically Synthesized Chalcopyrite $CuInS_2$ Nanoparticles. *Chem. Phys. Lett.* **2008**, *466*, 176−180.
(27) Cadirci, M.; Masala, O.; Pickett, N.; Binks, D. Ultrafast Charge Dynamics in $CuInS_2$ Nanocrystal Quantum Dots. *Chem. Phys.* **2014**, *438*, 60−65.
(28) Knowles, K. E.; Nelson, H. D.; Kilburn, T. B.; Gamelin, D. R. Singlet−Triplet Splittings in the Luminescent Excited States of Colloidal Cu^+:CdSe, Cu^+:InP, and $CuInS_2$ Nanocrystals: Charge-Transfer Configurations and Self-Trapped Excitons. *J. Am. Chem. Soc.* **2015**, *137*, 13138−13147.
(29) Shabaev, A.; Mehl, M. J.; Efros, A. L. Energy Band Structure of $CuInS_2$ and Optical Spectra of $CuInS_2$ Nanocrystals. *Phys. Rev. B: Condens. Matter Mater. Phys.* **2015**, *92*, 035431.
(30) Knowles, K. E.; Hartstein, K. H.; Kilburn, T. B.; Marchioro, A.; Nelson, H. D.; Whitham, P. J.; Gamelin, D. R. Luminescent Colloidal Semiconductor Nanocrystals Containing Copper: Synthesis, Photophysics, and Applications. *Chem. Rev.* **2016**, DOI: 10.1021/acs.chemrev.6b00048.
(31) Rice, W. D.; Mcdaniel, H.; Klimov, V. I.; Crooker, S. A. Magneto-Optical Properties of $CuInS_2$ Nanocrystals. *J. Phys. Chem. Lett.* **2014**, *5*, 4105−4109.

DOI: 10.1021/acs.jpclett.6b01668
J. Phys. Chem. Lett. 2016, 7, 3503−3509

(32) Huang, L.; Zhu, X.; Publicover, N. G.; Hunter, K. W.; Ahmadiantehrani, M.; de Bettencourt-Dias, A.; Bell, T. W. Cadmium and Zinc-Alloyed Cu-In-S Nanocrystals and Their Optical Properties. *J. Nanopart. Res.* **2013**, *15*, 2056.
(33) Kim, H.; Han, J. Y.; Kang, D. S.; Kim, S. W.; Jang, D. S.; Suh, M.; Kirakosyan, A.; Jeon, D. Y. Characteristics of $CuInS_2$/ZnS Quantum Dots and Its Application on LED. *J. Cryst. Growth* **2011**, *326*, 90−93.
(34) Choi, H. S.; Kim, Y.; Park, J. C.; Oh, M. H.; Jeon, D. Y.; Nam, Y. S. Highly Luminescent, Off-Stoichiometric $Cu_xIn_yS_2$/ZnS Quantum Dots for Near-Infrared Fluorescence Bio-Imaging. *RSC Adv.* **2015**, *5*, 43449−43455.
(35) Uehara, M.; Watanabe, K.; Tajiri, Y.; Nakamura, H.; Maeda, H. Synthesis of $CuInS_2$ Fluorescent Nanocrystals and Enhancement of Fluorescence by Controlling Crystal Defect. *J. Chem. Phys.* **2008**, *129*, 134709.
(36) Nose, K.; Soma, Y.; Omata, T.; Otsuka-Yao-Matsuo, S. Synthesis of Ternary $CuInS_2$ Nanocrystals; Phase Determination by Complex Ligand Species. *Chem. Mater.* **2009**, *21*, 2607−2613.
(37) Park, J.; Kim, S.-W. $CuInS_2$/ZnS Core/Shell Quantum Dots by Cation Exchange and Their Blue-Shifted Photoluminescence. *J. Mater. Chem.* **2011**, *21*, 3745−3750.
(38) Kim, Y.-K.; Ahn, S.-H.; Choi, G.-C.; Chung, K.-C.; Cho, Y.-S.; Choi, C.-J. Photoluminescence of $CuInS_2$/(Cd,Zn)S Nanocrystals as a Function of Shell Composition. *Trans. Electr. Electron. Mater.* **2011**, *12*, 218−221.
(39) Li, L.; Daou, T. J.; Texier, I.; Kim Chi, T. T.; Liem, N. Q.; Reiss, P. Highly Luminescent $CuInS_2$/ZnS Core/Shell Nanocrystals: Cadmium-Free Quantum Dots for In Vivo Imaging. *Chem. Mater.* **2009**, *21*, 2422−2429.
(40) Bose, R.; Ahmed, G. H.; Alarousu, E.; Parida, M. R.; Abdelhady, A. L.; Bakr, O. M.; Mohammed, O. F. Direct Femtosecond Observation of Charge Carrier Recombination in Ternary Semiconductor Nanocrystals: The Effect of Composition and Shelling. *J. Phys. Chem. C* **2015**, *119*, 3439−3446.
(41) Debnath, T.; Maiti, S.; Maity, P.; Ghosh, H. N. Subpicosecond Exciton Dynamics and Biexcitonic Feature in Colloidal $CuInS_2$ Nanocrystals: Role of In−Cu Antisite Defects. *J. Phys. Chem. Lett.* **2015**, *6*, 3458−3465.
(42) Sun, J.; Zhu, D.; Zhao, J.; Ikezawa, M.; Wang, X.; Masumoto, Y. Ultrafast Carrier Dynamics in $CuInS_2$ Quantum Dots. *Appl. Phys. Lett.* **2014**, *104*, 023118.
(43) Sakamoto, M.; Chen, L.; Okano, M.; Tex, D. M.; Kanemitsu, Y.; Teranishi, T. Photoinduced Carrier Dynamics of Nearly Stoichiometric Oleylamine-Protected Copper Indium Sulfide Nanoparticles and Nanodisks. *J. Phys. Chem. C* **2015**, *119*, 11100−11105.
(44) Jaffe, J.; Zunger, A. Electronic Structure of the Ternary Chalcopyrite Semiconductors $CuAlS_2$, $CuGaS_2$, $CuInS_2$, $CuAlSe_2$, $CuGaSe_2$, and $CuInSe_2$. *Phys. Rev. B: Condens. Matter Mater. Phys.* **1983**, *28*, 5822−5847.
(45) Guyot-Sionnest, P.; Hines, M. A. Intraband Transitions in Semiconductor Nanocrystals. *Appl. Phys. Lett.* **1998**, *72*, 686−688.
(46) Look, D. C.; Manthuruthil, J. C. Electron and Hole Conductivity in $CuInS_2$. *J. Phys. Chem. Solids* **1976**, *37*, 173−180.
(47) Jones, M.; Kumar, S.; Lo, S. S.; Scholes, G. D. Exciton Trapping and Recombination in Type II CdSe/CdTe Nanorod Heterostructures. *J. Phys. Chem. C* **2008**, *112*, 5423−5431.
(48) Whitham, P. J.; Marchioro, A.; Knowles, K. E.; Kilburn, T. B.; Reid, P. J.; Gamelin, D. R. Single-Particle Photoluminescence Spectra, Blinking, and Delayed Luminescence of Colloidal $CuInS_2$ Nanocrystals. *J. Phys. Chem. C* **2016**, *120*, 17136−17142.
(49) de Jong, M.; Seijo, L.; Meijerink, A.; Rabouw, F. T. Resolving the Ambiguity in the Relation between Stokes Shift and Huang−Rhys Parameter. *Phys. Chem. Chem. Phys.* **2015**, *17*, 16959−16969.
(50) Orlinskii, S. B.; Schmidt, J.; Baranov, P. G.; Hofmann, D. M.; de Mello Donegá, C.; Meijerink, A. Probing the wave function of shallow Li and Na donors in ZnO nanoparticles. *Phys. Rev. Lett.* **2004**, *92*, 047603.
(51) Baranov, P. G.; Orlinskii, S. B.; de Mello Donega, C.; Schmidt, J. High-frequency EPR and ENDOR spectroscopy on semiconductor quantum dots. *Appl. Magn. Reson.* **2010**, *39*, 151−183.
(52) Abrahams, S. C.; Bernstein, J. L. Piezoelectric Nonlinear Optic $CuGaS_2$ and $CuInS_2$ Crystal Structure: Sublattice Distortion in $A^IB^{III}C_2^{VI}$ and $A^{II}B^{IV}C_2^{V}$ Type Chalcopyrites. *J. Chem. Phys.* **1973**, *59*, 5415−5420.
(53) Jumpertz, E. A. Electron-Density Distribution in Zinc Blende. *Zeitschrift fuer Elektrochemie* **1955**, *59*, 419−425.
(54) Mueller, W. J.; Loeffler, G. Zur Kenntnis Der Faerbung von Gefaelltem Cadmiumsulfid. *Angew. Chem.* **1933**, *46*, 538−539.
(55) Stallworth, P. E.; Guillemoles, J. F.; Flowers, J.; Vedel, J.; Greenbaum, S. G. NMR Studies of $CuInS_2$ and $CuInSe_2$ Crystals Grown by the Bridgman Method. *Solid State Commun.* **2000**, *113*, 527−532.

DOI: 10.1021/acs.jpclett.6b01668
J. Phys. Chem. Lett. 2016, 7, 3503−3509